# Undulating rolls and their instabilities in a Rayleigh-Bénard layer

M. A. Zaks
*AG ''Nichtlineare Dynamik,'' Universität Potsdam, D-14415 Potsdam, Germany*

M. Auer and F. H. Busse
*Physikalisches Institut, Universität Bayreuth, D-95440 Bayreuth, Germany*

(Received 10 October 1995)

It has recently become apparent that undulating rolls and modulated undulating rolls represent physically realizable steady solutions of Rayleigh-Bénard convection in the neighborhood of the critical value of the Rayleigh number in addition to the solution of two-dimensional rolls. The relative regions of stability of these three types of convection are studied through analytical as well as through numerical methods. Symmetric stress-free as well as no-slip boundary conditions are considered; in the former case the analysis is restricted to moderate and high values of the Prandtl number. [S1063-651X(96)01005-7]

PACS number(s): 47.20.Bp, 47.20.Ky, 47.20.Lz, 47.54.+r

## I. INTRODUCTION

Undulating convection rolls have been seen in fluid layers heated from below in the presence of a mean flow or of other effects introducing anisotropies. In experiments by Avsec and Luntz [1] and by Bénard and Avsec [2] the onset of convection in an air layer with a mean Poiseuille flow has been visualized with tobacco smoke and undulating rolls aligned in the direction of the mean flow have been photographed. Later undulating rolls as a typical form of convection have been seen in inclined convection layers [3] and in electrohydrodynamic convection in liquid crystals [4]. The wavy instability of longitudinal straight rolls leading to the establishment of undulating rolls has been studied theoretically in the case of convection with a plane Couette shear [5] and in the case of an inclined convection layer [6]. More recently these studies have been extended to the case of convection in the presence of Poiseuille flow [7]. Investigations of undulating roll patterns in the case of electrohydrodynamic convection in liquid crystals have been made by Bodenschatz *et al.* [8]. For a recent review of the extensive research on convection in the presence of a mean shear we refer to Kelly [9].

The wavy instability of convection rolls occurs also in the horizontally isotropic case of a Rayleigh-Bénard layer where it is known as the zigzag instability [10,11]. But since the stability boundary in the plane spanned by the Rayleigh number $R$ and the wave number $\alpha$ never intersects the critical value $\alpha_c$ of $\alpha$, the transition to undulating rolls is usually not observed in experiments on convection rolls in the absence of anisotropic effects. In fact, it was long believed [12] that the zigzag instability has the sole purpose of facilitating the transition of rolls with a wavelength $\lambda$ exceeding the critical value $\lambda_c = 2\pi/\alpha_c$ by a certain finite amount to a set of new rolls oblique to the original ones with the wavelength $\lambda_c$. The experiments of Busse and Whitehead [13] have supported this idea in that rolls with fairly large values of $\lambda$ which were generated through the use of controlled initial conditions exhibited this transition. While this interpretation of the zigzag instability is still roughly applicable, more recent research [14] has indicated intermediate convection states which can eventually be realized experimentally in a sufficiently detailed study. In the present paper the surprisingly complex interaction between rolls of different orientations is revisited and the stability of undulating roll states and their modulations is analyzed with analytical and numerical methods.

The paper starts in Sec. II with a brief formulation of the mathematical problem. In Sec. III we follow the bifurcation scenario within the framework of the Newell-Whitehead-Segel equation. Instabilities with respect to long-wavelength pattern modulations are considered in Sec. IV. In Sec. V a bifurcation analysis of convection patterns in a fixed horizontal periodicity interval is described. In Sec. VI the analysis is extended further with the help of numerical methods. A general discussion of the results and a comparison with some older experimental observations is given in the concluding section.

## II. FORMULATION OF THE PROBLEM

We consider convection in a horizontal fluid layer of height $h$ heated from below with either no-slip or stress-free boundaries. The temperatures $T_1$ and $T_2$ are prescribed at the lower and upper boundaries, respectively. Using $h$ as length scale, $h^2/\kappa$ as time scale, where $\kappa$ is the thermal diffusivity, and $T_2 - T_1$ as temperature scale, the equations of motion for the velocity vector $\mathbf{v}$ and the heat equation for the deviation $\Theta$ of the temperature from its static distribution can be written in the form

$$P^{-1}\left(\frac{\partial}{\partial t}\mathbf{v} + \mathbf{v}\cdot\nabla\mathbf{v}\right) = -\nabla\Pi + R\Theta\mathbf{k} + \nabla^2\mathbf{v},$$

$$\nabla\cdot\mathbf{v} = 0, \tag{2.1}$$

$$\frac{\partial}{\partial t}\Theta + \mathbf{v}\cdot\nabla\Theta = \mathbf{v}\cdot\mathbf{k} + \nabla^2\Theta,$$

where the Rayleigh number $R$ and the Prandtl number $P$ are defined in the usual way,

 

$$R=\frac{\gamma(T_2-T_1)gh^3}{\nu\kappa},\quad P=\frac{\nu}{\kappa},\tag{2.2}$$

with the coefficient $\gamma$ of thermal expansion, the kinematic viscosity $\nu$, and the acceleration $g$ of gravity. It is convenient to use a Cartesian system of coordinates $x$, $y$, $z$ with $z$ in the direction of the vertical unit vector $\mathbf{k}$. The boundary conditions are then given either by

$$\Theta=v_z=\frac{\partial^2 v_z}{\partial z^2}=0$$

$$\text{for stress-free boundaries at } z=\pm\tfrac{1}{2},\tag{2.3a}$$

or by

$$\Theta=v_z=\frac{\partial v_z}{\partial z}=0$$

$$\text{for no-slip boundaries at } z=\pm\tfrac{1}{2}.\tag{2.3b}$$

Simple solutions of Eq. (2.1) of small amplitude which are periodic with the horizontal periodicity interval $0\leqslant x\leqslant 2\pi/\alpha$, $0\leqslant y\leqslant 2\pi/\beta$ can be written in the form

$$v_z=\sum_{j=-3}^{3}A_j f(z,|\mathbf{k}_j|)\exp\{i\mathbf{k}_j\cdot\mathbf{r}\}+\sum_{i,j=-3}^{3}A_iA_jF(z,\mathbf{k}_i\cdot\mathbf{k}_j)\times\exp\{i(\mathbf{k}_i+\mathbf{k}_j)\cdot\mathbf{r}\}+(\text{higher-order terms}),\tag{2.4}$$

where the horizontal vectors $\mathbf{k}_i$ are given by

$$\mathbf{k}_1=(\alpha,0,0),\quad \mathbf{k}_{2,3}=(\alpha,\pm\beta,0)$$

and where the relationships $\mathbf{k}_{-i}=-\mathbf{k}_i$ and $A_{-i}=A_i^*$ hold, with the star denoting the complex conjugate. Solutions describing convection patterns in the form of rolls, undulating rolls, rectangles, and oblique rolls can be represented by expression (2.4) as long as the control parameter $\varepsilon\equiv(R-R_c)/R_c$ is small in comparison with unity and the wave numbers $k_i\equiv|\mathbf{k}_i|$ do not differ much from the critical value $\alpha_c$ at which the Rayleigh number $R$ reaches its minimum value $R_c$.

According to Ref. [10], two-dimensional rolls of the form (2.4) with two of the three amplitudes $A_1, A_2, A_3$ vanishing are the only possibly stable solution among all steady solutions of Eq. (1) in the region

$$\xi_0^2(k-\alpha_c)^2\leqslant\varepsilon\left[1+\frac{P^2}{4(1+P)}\right],$$

$$\text{with } k>\alpha_c \text{ for stress-free conditions,}\tag{2.5a}$$

$$k-\alpha_c\leqslant -c(P)\varepsilon \quad \text{for no-slip conditions,}\tag{2.5b}$$

where $c$ is a positive constant depending on the Prandtl number and where $\xi_0^2$ is defined by $[d^2R(k)/dk^2]_{k=\alpha_c}/R_c$. The stability boundaries in the $\varepsilon$-$k$ plane corresponding to the equality sign in (2.5) describe the onset of the zigzag instability. This instability was described in Ref. [10], but the stability boundary given in this reference agrees with (2.5a) only in the limit of infinite $P$ and with (2.5b) only in the approximation of a vanishing $c(P)$. A finite value of $c$ was advocated in Ref. [15] and numerical determinations of the zigzag instability boundary have been provided in Refs. [11, 16]. The explicit expression

$$c(P)=\frac{0.033\,61+4.6669P^{-1}+1.2551P^{-2}}{0.699\,27-0.004\,72P^{-1}+0.008\,32P^{-2}}\tag{2.5c}$$

has been derived in Ref. [17]. Siggia and Zippelius [18] were the first to derive the correct stability boundary (2.5a) by taking into account the large scale mean flow induced in the presence of stress-free boundaries.

In order to describe the undulating rolls evolving from the zigzag instability in the regions (2.5) and to consider the stability properties of the latter type of solutions we shall use two different approaches. On the one hand it is convenient to use the formalism of the Newell-Whitehead-Segel equation since the zigzag instability is a long-wavelength instability of convection rolls. The other approach relies on amplitude equations for the amplitudes $A_i$ and allows one to express the stability boundaries in terms of the Prandtl and Rayleigh numbers. The long-wave disturbance approximation is not needed in this approach, but the solution of the amplitude equations usually requires a numerical treatment. To take into account the peculiarities of the stress-free case, we incorporate into our analysis of Sec. V the amplitude $u$ of the mean flow.

## III. BIFURCATIONS IN THE NEWELL-WHITEHEAD-SEGEL EQUATION

To provide the general description of the various patterns and their instabilities, it is convenient to use the formalism of amplitude equations. As long as the considered patterns remain close to straight rolls, one may use the Newell-Whitehead-Segel (NWS) amplitude equation [19,20] for the slowly varying complex amplitude of the rolls. After an appropriate rescaling the NWS equation can be written in the form

$$\frac{\partial U}{\partial t}=\left[\varepsilon-|U|^2+\left(\frac{\partial}{\partial x}-\frac{i}{2\eta}\frac{\partial^2}{\partial y^2}\right)^2\right]U,\tag{3.1}$$

where $\varepsilon$ denotes the control parameter and where $\eta$ is defined by $\eta=\alpha_c\xi_0^{-1}$. We shall concentrate on spatially periodic solutions with the roll wave number $q$ (which in terms of the convection pattern is the normalized difference from the critical wave number) and with the wave number $p(p\ll q)$ characterizing the modulation of the rolls along their axis:

$$U=A(t)\exp\{iqx\}+B(t)\exp\{i(qx-py)\}+C(t)\exp\{i(qx+py)\}+(\text{higher-order terms}).\tag{3.2}$$

Given the modulation scale $p^{-1}$, we can rescale $q$ and $\varepsilon$, $q=\tilde{q}p^2\eta^{-1}$ and $\varepsilon=\tilde{\varepsilon}p^4\eta^{-2}$, such that $\tilde{\varepsilon}=\varepsilon(\tilde{q}/q)^2$. In the analysis below the stability boundaries will be expressed in terms of the rescaled variables $\tilde{\varepsilon}$ and $\tilde{q}$.

By standard projection technique one obtains after discarding the terms of higher order (which means the assump-

tion of the smallness of $|B|$ and $|C|$ as compared to $|A|$) the equations for the time evolution of the complex amplitudes $A,B,C$:

$$\frac{dA}{dt}=A(l_A-|A|^2-2|B|^2-2|C|^2)-2A^*BC,$$

$$\frac{dB}{dt}=B(l_B-2|A|^2-|B|^2-2|C|^2)-A^2C^*, \qquad (3.3)$$

$$\frac{dC}{dt}=C(l_C-2|A|^2-2|B|^2-|C|^2)-A^2B^*,$$

with the linear increments $l_A=\varepsilon-q^2$ and $l_B=l_C=\varepsilon-(q+p^2/2\eta)^2$, both of which grow with increasing $\tilde{\varepsilon}$. The trigonometric representation of the variables $A=|A|\exp(i\omega_A)$, $B=|B|\exp(i\omega_B)$, $C=|C|\exp(i\omega_C)$ casts Eq. (3.3) into the form

$$\begin{aligned}\frac{d|A|}{dt}&=|A|[l_A-|A|^2-2|B|^2-2|C|^2\\&\quad-2|B||C|\cos(\omega_B+\omega_C-2\omega_A)],\\\frac{d|B|}{dt}&=|B|(l_B-2|A|^2-|B|^2-2|C|^2)\\&\quad-|A|^2|C|\cos(\omega_B+\omega_C-2\omega_A),\\\frac{d|C|}{dt}&=|C|(l_C-2|A|^2-2|B|^2-|C|^2)\\&\quad-|A|^2|B|\cos(\omega_B+\omega_C-2\omega_A),\end{aligned} \qquad (3.4)$$

$$\frac{d}{dt}(\omega_B+\omega_C-2\omega_A)=-\sin(\omega_B+\omega_C-2\omega_A)\times\left[|A|^2\left(\frac{|B|^2}{|C|^2}+\frac{|C|^2}{|B|^2}\right)+2|B||C|\right].$$

The dependence of the dynamics on the combination $\omega_B+\omega_C-2\omega_A\equiv\omega_{ABC}$ instead of the individual phases is owed to the symmetry of the problem with respect to translations in both the $x$ and $y$ directions. It can be easily seen from the last of Eqs. (3.4) that in the generic case (when the initial value of $\omega_{ABC}$ is not an even multiple of $\pi$) this combination monotonically approaches the nearest odd multiple of $\pi$, with $\cos(\omega_{ABC})\to-1$, i.e., the complex variables are getting phase locked. Moreover, insofar as the time derivative of each individual phase is also proportional to the eventually vanishing $\sin\omega_{ABC}$, there can be no ''corotation'' of variables (which would correspond to a traveling wave) inside this locked state: each of the phases tends to a constant value. Since we are interested in the properties of the final states only, we may treat the equations as real ones without reducing the generality:

$$\frac{dA}{dt}=A(l_A-A^2-2B^2-2C^2+2BC),$$

$$\frac{dB}{dt}=B(l_B-2A^2-B^2-2C^2)+A^2C, \qquad (3.5)$$

$$\frac{dC}{dt}=C(l_C-2A^2-2B^2-C^2)+A^2B.$$

The dynamics of the system (3.5) is bounded, i.e., the value of

$$\frac{d(A^2+B^2+C^2)}{dt}=2(l_AA^2+l_BB^2+l_CC^2)-4A^2(B-C)^2-2(A^2+B^2+C^2)-4B^2C^2 \qquad (3.6)$$

is obviously negative for large values of $|A|$, $|B|$, or $|C|$. At the same time this system inherits from the Newell-Whitehead-Segel equation the variational property

$$\frac{d}{dt}\left(-\frac{1}{2}(l_AA^2+l_BB^2+l_CC^2)+\frac{1}{4}(A^4+B^4+C^4)+A^2B^2+A^2C^2+B^2C^2-A^2BC\right)=-\left(\frac{dA}{dt}\right)^2-\left(\frac{dB}{dt}\right)^2-\left(\frac{dC}{dt}\right)^2\leqslant 0. \qquad (3.7)$$

The combination of the two latter properties implies that the only possible global attractors of (3.5) are the stationary solutions. One should also notice in (3.5) the presence of the invariant subspaces $C=B$ and $C=-B$.

The basic pattern, the proximity to which is necessary for the validity of the Newell-Whitehead-Segel approach, is the pattern of rolls parallel to the $y$ axis. The corresponding fixed points have the coordinates $\{A,B,C\}=\{l_A^2,0,0\}$ and will be referred to as ''$A$ rolls.'' Other possible pure roll solutions are those in which only the $B$ or the $C$ mode is excited ($B$ and $C$ rolls, respectively). We are interested in the parameter values for which the $A$ rolls are unstable with respect to zigzag perturbations; this corresponds to the condition $l_B>l_A$, which defines in the $\tilde{q}$-$\tilde{\varepsilon}$ plane the half plane

$$\tilde{q}\leqslant-\tfrac{1}{4} \qquad (3.8)$$

whose vertical right boundary separates the domain of zigzag-stable rolls from that of the long-wave zigzag-unstable ones. In the following we shall restrict ourselves to the domain (3.8). As a consequence the $A$ rolls always have at least one growing perturbation mode. Aiming at the complete description of the bifurcations of the steady solutions of Eq. (3.5) the condition of smallness of $|B|$ and $|C|$ as compared to $|A|$ will be waived.

When both $l_A$ and $l_B$ are negative, the only attracting state is the trivial zero equilibrium. With increasing $\tilde{\varepsilon}$, $l_B$ becomes positive for $\tilde{\varepsilon}\geqslant\tilde{\varepsilon}_B=(\tilde{q}+\frac{1}{2})^2$ and two symmetric couples of stable $B$ rolls ($B^2=l_B$) and $C$ rolls ($C^2=l_B$) bifurcate from

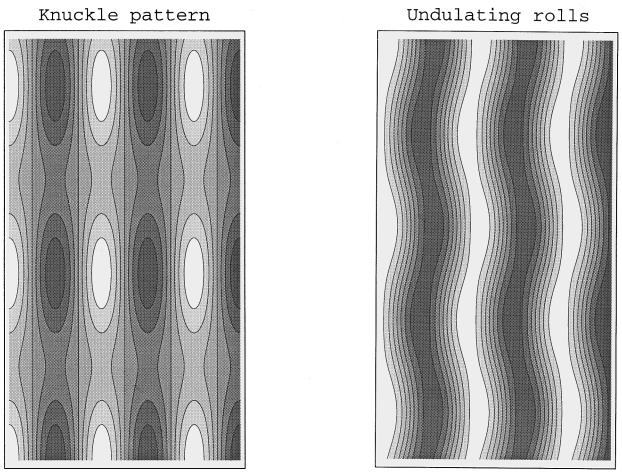


FIG. 1. Patterns of solutions bifurcating from straight rolls: knuckle pattern (left) and undulating rolls (right). The patterns have been obtained through a superposition of disturbances with a finite amplitude onto the pattern of straight rolls.

zero. Their basins of attraction in the phase space are separated by the stable manifolds of the simultaneously born unstable fixed points, given by the expression $A=0$, $B^2=C^2=l_B/3$, and corresponding to the rectangle patterns. At $l_A=0$ ($\tilde{\varepsilon}=\tilde{\varepsilon}_A=\tilde{q}^2$) the couple of unstable $A$ rolls bifurcates from zero; these fixed points have two positive eigenvalues. The two corresponding eigenmodes describe modulations of the roll boundaries with the excursions of the opposite boundaries being either in counterphase (the ''knuckle'' instability) or in phase (the ''zigzag'' instability) as shown in Fig. 1. The knuckle instability is removed through the subcritical pitchfork bifurcation occurring at the line $l_B=3l_A$, which in terms of the coefficients of the initial problem is given by

$$\tilde{\varepsilon}=\tilde{\varepsilon}_K=\tilde{q}^2-\frac{\tilde{q}}{2}-\frac{1}{8}. \tag{3.9}$$

The mixed-mode solutions with $A^2=(2l_B-l_A)/5$, $B^2=(3l_A-l_B)/15$, $C=-B$, which are born at this bifurcation and exist for $\tilde{\varepsilon}>\tilde{\varepsilon}_K$, are always unstable due to the presence of two positive eigenvalues $\lambda$ corresponding to growth rates of disturbances: one of them equals $2l_B/3$ and is responsible for the breaking of the symmetry $C=-B$; the other one is the positive root of the characteristic equation $5\lambda^2+2(2l_A+l_B)\lambda-20A^2B^2=0$ which describes the perturbations within the subspace $C=-B$.

The zigzag instability in the case of $A$ rolls is stabilized only at the right boundary $l_A=l_B$ of the domain (3.8). As a result of this supercritical pitchfork bifurcation the steady solutions with

$$A^2=3l_A-2l_B, \quad B^2=l_B-l_A, \quad C=B \tag{3.10}$$

are born which correspond to the undulating roll pattern. Thus the right boundary of the domain in which the pattern (3.10) exists is given by $l_A=l_B$; the left one is the line $3l_A=2l_B$, i.e.,

$$\tilde{\varepsilon}=\tilde{\varepsilon}_U=\tilde{q}^2-2\tilde{q}-\tfrac{1}{2}. \tag{3.11}$$

The condition $\tilde{\varepsilon}=\tilde{\varepsilon}_U$ corresponds to the supercritical pitchfork bifurcation, at which the solutions (3.10) branch from the unstable rectangular pattern. Along with two obviously negative eigenvalues corresponding to the invariant subspace $B=C$ (the characteristic equation being $\lambda^2+2l_B\lambda+4A^2B^2=0$), the solutions (3.10) possess the eigenvalue $6l_B-8l_A$ which is responsible for the eigenmode with $B\neq C$ and is positive close to $\tilde{\varepsilon}_U$, but becomes negative for

$$\tilde{\varepsilon}\geqslant\tilde{\varepsilon}_S=\tilde{q}^2-3\tilde{q}-\tfrac{3}{4}, \tag{3.12}$$

which condition defines the domain of stability of the undulating rolls. The line $\tilde{\varepsilon}=\tilde{\varepsilon}_S$ denotes the subcritical pitchfork bifurcation, at which the unstable steady mixed-mode solutions

$$B^2=\frac{l_B}{(1+\rho)^2}, \quad A^2=\rho B^2, \quad C=\rho B,$$

$$\text{where} \quad \rho^2+\rho\,\frac{2l_A+l_B}{l_A-2l_B}+1=0 \tag{3.13}$$

are born which exist for $\tilde{\varepsilon}\geqslant\tilde{\varepsilon}_S$. The bifurcation at (3.12) is a symmetry-breaking bifurcation: unlike the undulating rolls (3.10), the unstable solutions (3.13) do not possess reflectional symmetry in the longitudinal direction.

For fixed $\tilde{q}$ the bifurcation values of $\tilde{\varepsilon}$ are ordered in the following way: $0<\tilde{\varepsilon}_B<\tilde{\varepsilon}_A<\tilde{\varepsilon}_T<\tilde{\varepsilon}_U<\tilde{\varepsilon}_S$. To summarize, let us consider the route across the domain (3.8) which corresponds to an increase of both $\tilde{q}$ and $\tilde{\varepsilon}$. After the destabilization of the zero equilibrium one observes the birth of stable $B$ and $C$ rolls as well as of unstable rectangles. Later the unstable $A$ rolls are born; their instability is partially remedied at the line $\tilde{\varepsilon}=\tilde{\varepsilon}_T$. Further on, the unstable undulating rolls are born from the rectangles at the line $\tilde{\varepsilon}=\tilde{\varepsilon}_U$. They get stabilized at the line $\tilde{\varepsilon}=\tilde{\varepsilon}_S$, emitting the unstable solutions (3.13). Finally, at the right boundary $\tilde{q}=-\frac{1}{4}$ the stable undulating rolls merge into the $A$ rolls, thus stabilizing them. For the case of fixed negative $\tilde{q}$ and varying $\tilde{\varepsilon}$ the interchange of stability between the steady states is sketched in Fig. 2, where the solid lines denote the stable states, whereas the dashed and dotted curves correspond to the unstable solutions with one and two positive eigenvalues, respectively.

## IV. LONG-WAVE MODULATIONAL INSTABILITIES OF THE UNDULATING ROLLS

The conclusion about the stability of the undulating rolls (3.10) for $\tilde{\varepsilon}>\tilde{\varepsilon}_S$ is valid only within the class of the patterns given by Eq. (3.2). To allow for perturbations modulating the wavelength of the pattern, let us impose onto (3.10) infinitesimal disturbances of the form

$$\sum_{\pm} \exp\{\pm id(x\cos\phi+y\sin\phi)\}[\xi_1^{\pm}\exp\{iqx\} + \xi_2^{\pm}\exp\{i(qx-py)\}+\xi_3^{\pm}\exp\{i(qx+py)\}]+\text{c.c.}, \tag{4.1}$$

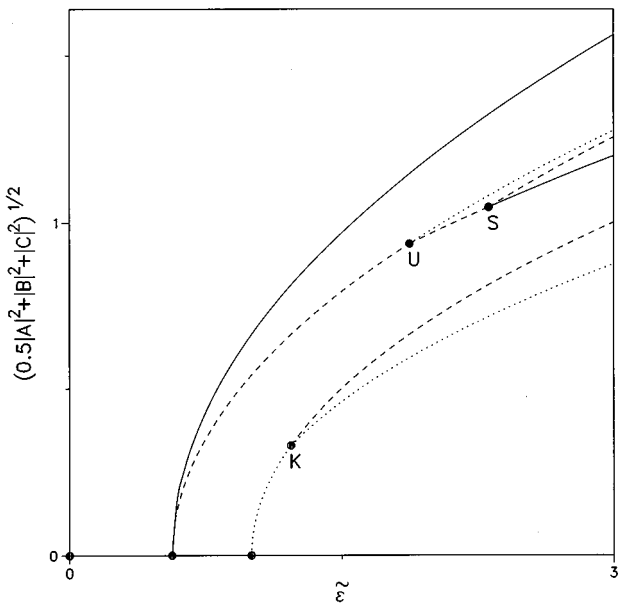


FIG. 2. Exchange of stability between bifurcating steady solutions for $\tilde{q}=-1.0$. Stable solutions are indicated by a solid line, unstable solutions with one (two) positive growth rates are indicated by dashed (dotted) lines. Circles mark pitchfork bifurcations. The circles denoted by $K,U,S$ correspond to the disappearance of the knuckle instability, the birth of undulating rolls from rectangles, and stabilization of undulating rolls through the emission of asymmetric mixed solutions, respectively.

where the angle $\phi(0<\phi<\pi/2)$ characterizes the direction of the modulation. The value of $d$ is assumed to be small as compared to $q$. After substituting this ansatz into the NWS equation one obtains the linearized equations for the dynamics of the amplitudes $\xi_j(t)$:

$$\begin{aligned}
\dot{\xi}_1^{\pm} &= \xi_1^{\pm}(l_1^{\pm}-4B^2-2A^2)+\xi_1^{\mp}{}^*(2B^2-A^2)-2\xi_2^{\mp}{}^*AB \\
&\quad +2\xi_3^{\mp}{}^*AB, \\
\dot{\xi}_2^{\pm} &= \xi_2^{\pm}(l_2^{\pm}-4B^2-2A^2)+2\xi_3^{\pm}B^2-2\xi_1^{\mp}{}^*AB-\xi_2^{\mp}{}^*B^2 \\
&\quad +\xi_3^{\mp}{}^*(2B^2-A^2), \\
\dot{\xi}_3^{\pm} &= 2\xi_2^{\pm}B^2+\xi_3^{\pm}(l_3^{\pm}-4B^2-2A^2)+2\xi_1^{\mp}{}^*AB \\
&\quad +\xi_2^{\mp}{}^*(2B^2-A^2)-\xi_3^{\mp}{}^*B^2,
\end{aligned} \tag{4.2}$$

where the values of $A$ and $B$ are taken from (3.10), and the coefficients $l_j^{\pm}$ $(j=1,2,3)$ represent the contributions of the linear term of the NWS equation to the dynamics of the modes $\xi_j^{+}$ and $\xi_j^{-}$ given by the formulas

$$\begin{aligned}
l_1^{\pm} &= \varepsilon-\left(\pm d\,\cos\phi+q+\frac{d^2\sin^2\phi}{2\eta}\right)^2, \\
l_2^{\pm} &= \varepsilon-\left(\pm d\,\cos\phi+q+\frac{(\pm d\,\sin\phi-p)^2}{2\eta}\right)^2, \\
l_3^{\pm} &= \varepsilon-\left(\pm d\,\cos\phi+q+\frac{(\pm d\,\sin\phi+p)^2}{2\eta}\right)^2.
\end{aligned} \tag{4.3}$$

The growth rates $\lambda_j$ of the eigenmodes $\xi^{\pm}(t)\propto\exp(\lambda t)$ of Eq. (4.2) can be found as the eigenvalues of the corresponding complex matrix of sixth order. Owing to the fact that the coefficients of (4.2) are real, the latter matrix is decomposed into two identical real matrices, which are associated with the real and imaginary components of the amplitudes $\xi_j^{\pm}$, respectively. In fact, this separation means that all the eigenvalues of the complex matrix (which are real due to the variational property of the NWS equation) must be of multiplicity not less than 2. This additional symmetry arises from the freedom of choice of the phase of the complex perturbation. Due to this degeneracy the pitchfork bifurcation should produce not a couple of new steady solutions but a continuous family of them (parametrized by the phase). If the corresponding symmetry is disturbed, the family disappears, leaving isolated fixed points since oscillatory states like standing or traveling waves are forbidden by the variational character of dynamics. Keeping this in mind, we will simply consider below the real matrix of sixth order which can be, for example, the one acting in the subspace of the real parts of $\xi_j^{+}$ and $\xi_j^{-}$.

Further reductions are possible when the problem has additional symmetries. These are encountered when the modulation is directed either along the $x$ axis $(\phi=0)$ or along the $y$ axis $(\phi=\pi/2)$, respectively. Let us consider the first of these two possibilities. In this case $l_2^{+}=l_3^{+}$ and $l_2^{-}=l_3^{-}$ holds, and the matrix of the sixth order can be further decomposed into two submatrices. The first of them is responsible for the four-dimensional invariant subspace defined by the conditions $\xi_2^{\pm}=-\xi_3^{\pm}$, and the second one corresponds to the two-dimensional invariant plane $\xi_2^{\pm}-\xi_3^{\pm}=\xi_1^{\pm}=0$. The determinant of the related matrix for the perturbations of the former kind [the ''domain'' perturbations, see Fig. 3(a)] can be presented as

$$\begin{aligned}
&8d^2A^2B^2\,\frac{p^4}{\eta^2}\,(\tilde{\varepsilon}-3\tilde{q}^2-1)+d^4K_4(\tilde{\varepsilon},\tilde{q}) \\
&\qquad +d^6K_6(\tilde{\varepsilon},\tilde{q})+d^8.
\end{aligned} \tag{4.4}$$

The stability of the undulated rolls with respect to the domain perturbations with vanishing $d$ requires the positiveness of the factor of $d^2$ in (4.4):

$$\tilde{\varepsilon}>\tilde{\varepsilon}_d=3\tilde{q}^2+1. \tag{4.5}$$

By inspection both factors $K_4$ and $K_6$ in (4.4) are positive for $\tilde{\varepsilon}\leqslant\tilde{\varepsilon}_d$ and $\tilde{q}<-\frac{1}{4}$. Consequently, the instability for finite $d$ arises for higher values of $\tilde{\varepsilon}$ than in the case of infinitesimal $d$.

Two growth rates $\lambda$ for the perturbations belonging to the second kind of symmetry [the corresponding flow pattern is shown in Fig. 3(b)] are determined from the characteristic equation

$$\begin{aligned}
&\lambda^2-2\lambda(B^2-A^2-d^2) \\
&\qquad +2d^2\left[B^2-A^2-2\left(q+\frac{p^2}{2\eta}\right)^2+d^2\right]=0.
\end{aligned} \tag{4.6}$$

Hence the stability condition

Fig. 3a

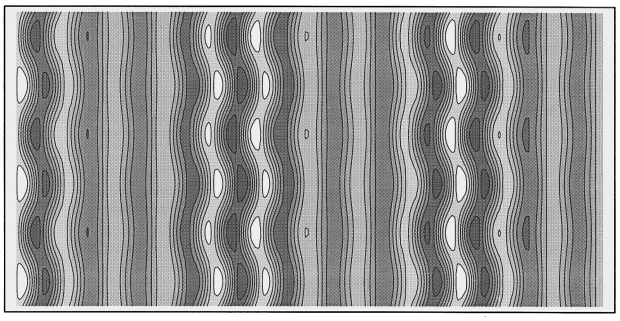

Fig. 3b

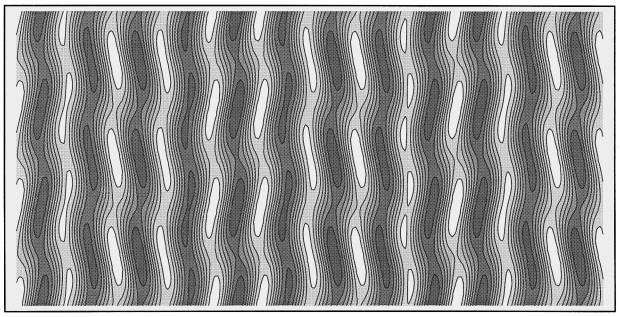

FIG. 3. Patterns of transversal long-wave instabilities of undulating rolls. The long-wave instability manifests itself either in modulation of the amplitude of undulations [(a), see also Ref. [14]] or in a modulation of the phase of undulations [(b)].

$$\tilde{\varepsilon} > \tilde{\varepsilon}_n \equiv 3\tilde{q}^2 - \tilde{q} - \frac{1}{4} - d^2 \frac{\eta^2}{p^4} \tag{4.7}$$

follows, which shows again that among all disturbances those with infinitesimal $d$ are the most dangerous.

Owing to the fact that both $\tilde{\varepsilon}_d$ and $\tilde{\varepsilon}_n$ are obviously larger than $\tilde{\varepsilon}_S$, these two instabilities reduce the domain of existence of stable undulating rolls. In the case of very small $d$ the value of $\tilde{\varepsilon}_n$ is smaller than that of $\tilde{\varepsilon}_d$ for $\tilde{q} > -\frac{5}{4}$. On the other hand, the patterns with $\tilde{q} < -\frac{5}{4}$ are more sensitive to the perturbations of the second kind.

Now let us consider the second special case: the modulations of the pattern (3.10) in the $y$ direction. In this situation $l_1^+ = l_1^-$, $l_2^+ = l_3^-$, and $l_2^- = l_3^+$. The Jacobian matrix of (4.2) is decomposed into two matrices of third order. The respective perturbations have basically the similar ribbonlike shape but differ by the phase, which is shifted along the undulated pattern by half of its transversal period. The first of the submatrices corresponds to the variables $\xi_1^+ + \xi_1^{-*}$, $\xi_2^+ - \xi_3^{-*}$, and $\xi_3^+ - \xi_2^{-*}$. For $d=0$ (when $l_2^{\pm} = l_3^{\pm} = l_B$ and $l_1^{\pm} = l_A$) it has two obviously negative eigenvalues equal to $-(3B^2+A^2) \pm \sqrt{(3B^2+A^2)^2 - 4A^2B^2}$ and the third eigenvalue equals zero. To evaluate the effect of a small, but finite $d$ on this last eigenvalue, the determinant of the matrix must be calculated with the result

$$\frac{A^2 p^6}{2\eta^4} (24\tilde{q}^2 + 30\tilde{q} + 7) d^2 + o(d^4). \tag{4.8}$$

The stability of the solutions (3.10) with respect to the perturbations with vanishing $d$ requires that the bracketed expression in the last expression should be negative, that is,

$$\frac{-15 - \sqrt{57}}{24} < \tilde{q} < \frac{-15 + \sqrt{57}}{24}. \tag{4.9}$$

It is noteworthy that this condition does not depend on $\tilde{\varepsilon}$ and imposes restrictions only on the wave number. The eigenvalues of the other third order matrix which describes the variables $\xi_1^+ - \xi_1^{-*}$, $\xi_2^+ + \xi_3^{-*}$, and $\xi_3^+ + \xi_2^{-*}$ at $d=0$ are 0, $-2(2B^2+A^2)$, $2(B^2-A^2)$. For $\tilde{\varepsilon} > \tilde{\varepsilon}_S$ the last one is negative, and the possible instability for small but finite values of $d$ can be associated only with the first eigenvalue. The determinant of the matrix equals

$$\frac{p^{10}}{\eta^6} \left( -4\tilde{q}\tilde{\varepsilon}^2 + \tilde{\varepsilon}(8\tilde{q}^3 - 12\tilde{q}^2 + 9\tilde{q} + 3) + \frac{5}{4} + 10\tilde{q} + 13\tilde{q}^2 - 25\tilde{q}^3 + 12\tilde{q}^4 - 4\tilde{q}^5 \right) d^2 + o(d^4). \tag{4.10}$$

The domain of stability of the solutions (3.10) with respect to the long-wave disturbances of the considered symmetry type is bounded by the curve at which the bracketed expression in (4.10) vanishes. This condition yields a quadratic equation for $\tilde{\varepsilon}$. In the region of existence of the undulating rolls ($\tilde{\varepsilon} < -\frac{1}{4}$) this equation has real roots only in the interval $-0.687\,15 < \tilde{q} < -0.294\,43$. Therefore the domain of stability is encircled by a closed curve $\tilde{\varepsilon} = \tilde{\varepsilon}_l$ stretched between these two values of $\tilde{q}$ (the upper and lower branches of the curve correspond to the two roots of the quadratic equation).

The bifurcation diagram in the $\tilde{q}$-$\tilde{\varepsilon}$ plane is presented in Fig. 4(a), where all described bifurcation lines are plotted. As a curious detail one may notice the tangency of three curves: $\tilde{\varepsilon}_S(\tilde{q})$, $\tilde{\varepsilon}_n(\tilde{q})$, and the lower branch of the curve $\tilde{\varepsilon}_l(\tilde{q})$ at the point ($\tilde{q} = -\frac{1}{2}$, $\tilde{\varepsilon} = 1$). However, the instabilities whose onset is marked by these curves, as well as those occurring outside the vertical stripe bounded by the lines (4.9), seem to be of purely academic significance. One sees that the undulating rolls given by the expression (3.10) are unstable with respect to long-wave disturbances almost everywhere in the region of their existence. The only exception is the narrow wedge between the two intersections of the curve $\tilde{\varepsilon}_d$ with the upper branch of the curve $\tilde{\varepsilon}_l$ which occur at the points ($\tilde{q} = -\frac{1}{2}$, $\tilde{\varepsilon} = \frac{7}{4}$) and ($\tilde{q} = -0.595\,03$, $\tilde{\varepsilon} = 2.0633$). In the application to the physical problem, of course, the rescaling $\varepsilon = \tilde{\varepsilon}(q/\tilde{q})^2$, $q = \tilde{q} p^2 \eta^{-1}$ has to be kept in mind.

The nonlinear development of the long-wave modulations may be estimated through the computation of the cubic terms in the corresponding amplitude expansions. Our calculations show that both of two relevant instabilities, encircling the mentioned island of stability of the undulated rolls, are supercritical: this means that the corresponding patterns should be stable at least locally near the respective bifurcation boundaries. Thus one may expect to observe the stable domainlike patterns immediately below the curve $\tilde{\varepsilon}_d$ and ribbonlike longitudinally modulated undulating rolls for $\tilde{\varepsilon} \geqslant \tilde{\varepsilon}_l$. Among the latter patterns those are of special interest whose

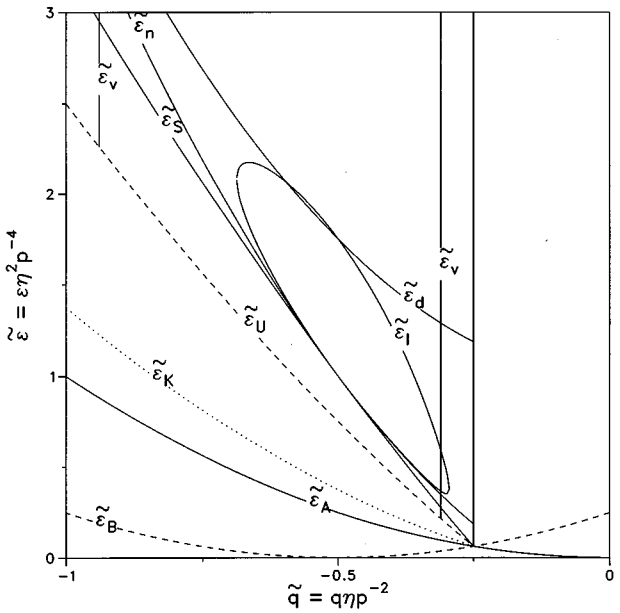


FIG. 4. Bifurcation diagram based on the Newell-Whitehead-Segel equation. $\tilde{\varepsilon}_B$, birth of stable $B$ and $C$ rolls and unstable rectangles; $\tilde{\varepsilon}_A$, birth of unstable $A$ rolls; $\tilde{\varepsilon}_K$, removal of the knuckle instability of $A$ rolls; $\tilde{\varepsilon}_U$, birth of unstable undulating rolls from rectangles; $\tilde{\varepsilon}_S$, stabilization of undulating rolls through symmetry breaking; $\tilde{\varepsilon}_d$, boundary of domain instability for undulating rolls; $\tilde{\varepsilon}_n$, stability boundary provided by Eq. (4.7); $\tilde{\varepsilon}_v$, stability lines given by Eq. (4.9); $\tilde{\varepsilon}_l$, boundary of the longitudinal modulation instability (4.10) for undulating rolls.

modulation length is in resonance with the wave number $p$ of the undulating rolls themselves. Two examples are shown in Fig. 5.

## V. BIFURCATIONS IN THE AMPLITUDE EXPANSION OF THE BOUSSINESQ EQUATIONS

The predictions obtained above with the help of the NWS equation can readily be applied for all Prandtl numbers to the case of convection in a fluid layer with rigid boundaries. The dynamical properties of a fluid layer with stress-free boundaries are still described by the NWS equation as long as the Prandtl number $P$ is infinite. When $P$ is finite, the effects due to the possible presence of a mean flow must be taken into account. In order to include the mean flow we perform the analysis for the stress-free case with the help of coupled amplitude equations describing the temporal evolution of the velocity field. This dynamical model captures reasonably well the basic phenomena close to the onset of convection. When the velocity field is decomposed into a poloidal and a toroidal component, $\mathbf{v}=\boldsymbol{\nabla}\times(\boldsymbol{\nabla}\times\mathbf{k}\Phi)+\boldsymbol{\nabla}\times\mathbf{k}\psi$ (where $\mathbf{k}$ is the vertical unit vector), then three complex variables, $a_j(t)$ $(j=1,2,3)$, correspond to the time-dependent amplitudes of the basic components of $\Phi$ whose wave vectors may be written in the form $\mathbf{k_j}=(\alpha,(j-2)p,0)$. Both the values of $p$ and of $\alpha_c-\alpha$ are assumed to be positive and small where $\alpha_c=\pi/\sqrt{2}$ is the critical wave number. The fourth variable $u(t)$ is responsible for the mean flow and corresponds to the component of the toroidal field with the weakest linear damping (it can be represented as a sum of two terms generated by the interaction of the first mode with the second one and the second mode with the third mode, respectively).

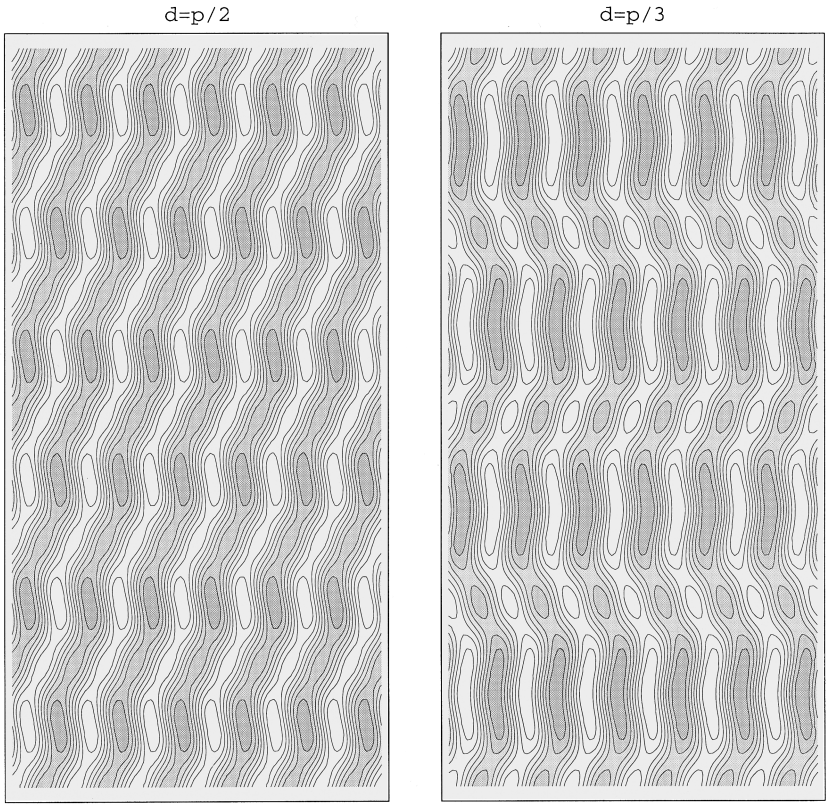


FIG. 5. Patterns of longitudinal modulations of the undulating rolls. The modulation wave number $d$ is a fraction of one-half (left pattern) or one-third (right pattern) of the wave number of the undulations.

The equations governing the time evolution of the amplitudes $a_j, u$ are

$$\dot{a}_1=\gamma_1(R-R_1)a_1-a_1\left(\sum_{i=1}^{3}\sigma_{1i}|a_i|^2\right)-\sigma_{14}a_2^2a_3^*+s_1a_2u^*,$$

$$\dot{a}_2=\gamma_2(R-R_2)a_2-a_2\left(\sum_{i=1}^{3}\sigma_{2i}|a_i|^2\right)-\sigma_{24}a_1a_2^*a_3+s_2(a_3u^*-a_1u),$$

$$\dot{a}_3=\gamma_3(R-R_3)a_3-a_3\left(\sum_{i=1}^{3}\sigma_{3i}|a_i|^2\right)-\sigma_{34}a_2^2a_1^*-s_1a_2u, \tag{5.1}$$

$$\dot{u}=-\delta^2u+Q(a_3a_2^*-a_2a_1^*),$$

where $R_j=(\pi^2+|k_j|^2)^3|k_j|^{-2}$ are the threshold values of $R$ corresponding to the excitation of the $j$th mode, $Q=\alpha p\pi^2/2$, and the factors $\gamma_j$ are given by $\gamma_j=|k_j|^2(\pi^2+|k_j|^2)^{-2}(1+P)^{-1}$. The derivation of Eq. (5.1) as well as the complicated expressions relating the factors $\sigma_{ij}$ and $s_i$ of the nonlinear terms to the parameters $R$, $P$, $\alpha$, and $p$ can be found in Ref. [21] where $\alpha,p$ are denoted by $\beta,\delta$. The symmetries displayed by the quadratic terms depend on the symmetry between $\mathbf{k}_1$ and $\mathbf{k}_3$. Besides the obvious consequence $R_1=R_3$, the latter symmetry also simplifies the matrix of the coefficients of the cubic terms: $\sigma_{11}=\sigma_{33}$, $\sigma_{12}=\sigma_{32}$, $\sigma_{13}=\sigma_{31}$, $\sigma_{14}=\sigma_{34}$, and $\sigma_{21}=\sigma_{23}$.

The basic difference between Eqs. (3.3) and (5.1) is the presence of the fourth component representing the mean flow. This term not only increases the order of the system but also destroys the variational character of the dynamics. In the general case it is impossible to prove that the only attractors are the steady solutions. On the contrary, it can be shown that at very low values of $P$ Hopf bifurcations will be encountered, giving rise to time dependency. However, at the high and moderate values of $P$ the influence of the mean flow is more quantitative than qualitative, and the assumption that, similarly to the case of the NWS equation, the whole phase space can be decomposed into the domains of attraction of the few fixed points (for which only the *local* stability can be proven) seems quite plausible.

Once again, the presentation in the trigonometric form $a_j=|a_j|\exp(i\omega_j)$ $(j=1,2,3)$, $u=|u|\exp(i\omega_4)$ permits us to reduce the actual dimension of the problem. Due to the two translational symmetries in the plane of the layer the dynamics does not depend on the individual values of $\omega_j$, but only on the combinations $\omega_1-2\omega_2+\omega_3$ and $\omega_2-\omega_1-\omega_4$. Although we are unable to prove that the union of invariant subspaces in which both of these combinations are even multiples of $\pi$ is globally attracting, our numerical experiments with different initial conditions strongly support this assumption. The time derivatives of individual phases $\omega_j$ are proportional to sines of the collective phases and thus vanish on these subspaces. The solutions with time-independent amplitudes for which the mentioned combinations are different from multiples of $\pi$ would describe traveling waves. These can be encountered only for rather low values of $P$ and are unstable for the considered wave vectors. The problem is thus reduced to the set of real ordinary differential equations:

$$\begin{aligned}
\dot{a}_1&=\gamma_1(R-R_1)a_1-a_1(\sigma_{11}a_1^2+\sigma_{12}a_2^2+\sigma_{13}a_3^2)-\sigma_{14}a_2^2a_3\\
&\quad+s_1a_2u,\\
\dot{a}_2&=\gamma_2(R-R_2)a_2-a_2(\sigma_{21}a_1^2+\sigma_{22}a_2^2+\sigma_{21}a_3^2+\sigma_{24}a_1a_3)\\
&\quad+s_2u(a_3-a_1),\\
\dot{a}_3&=\gamma_1(R-R_1)a_3-a_3(\sigma_{13}a_1^2+\sigma_{12}a_2^2+\sigma_{11}a_3^2)-\sigma_{14}a_2^2a_1\\
&\quad-s_1a_2u,\\
\dot{u}&=-\delta^2u+Qa_2(a_3-a_1).
\end{aligned} \tag{5.2}$$

We consider the bifurcations of steady states in Eqs. (5.2) under the provision $R_1<R_2$, which is equivalent to $p<(\pi^2+\alpha^2)(1+4\sqrt{1+4\pi^2\alpha^{-2}}-3)/2$. Having fixed the values of $P$, $\alpha$, and $p$ we increase the Rayleigh number beyond the threshold value $R_1$ which marks the onset of convection in the form of the roll pattern with the wave vector $\{\alpha,p\}$. In the general case the explicit expressions for the coefficients of (5.2) corresponding to each of the occurring bifurcations do not shed direct light on the respective interrelations between the bifurcational values of the physical parameters $R$, $P$, $\alpha$, and $p$, owing to the complicated way in which the former depend on the latter. A simplification is possible in the case of small $p$ for which the truncation employed for the velocity field provides the asymptotically correct description of the situation. The leading terms in the expansions for the coefficients are given in this case by the $R$-independent expressions:

$$\sigma_{12}=\sigma_{13}=\sigma_{21}=\sigma_{24}=2\sigma_{11}=2\sigma_{14}=2\sigma_{22}=\frac{\alpha^4P^2}{1+P}+o(p^2),$$

$$s_1=s_2=p[\alpha+o(p^2)],\quad \gamma_1=\gamma_2+o(p^2). \tag{5.3}$$

It turns out that in the range of high and moderate values of $P$ the increase of $R$ leads to the same sequence of bifurcations as the increase of $\tilde{\varepsilon}$ in the NWS equation for $\tilde{q}<-\frac{1}{4}$. At $R=R_1$ the mechanical equilibrium loses stability, and the stable rolls with $(a_1^2,a_2^2,a_3^2,u)=(\gamma_1(R-R_1)\sigma_{11}^{-1},0,0,0)$ and $(a_1^2,a_2^2,a_3^2,u)=(0,0,\gamma_1(R-R_1)\sigma_{11}^{-1},0)$ (the analogs of $B$ and $C$ rolls from the preceding section) are born. Their domains of attraction in the phase space are separated by the stable manifolds of the nonstable steady solutions with $a_1^2=a_3^2=\gamma_1(R-R_1)(\sigma_{11}+\sigma_{13})^{-1}$, $a_2=u=0$, which correspond to the unstable rectangular planforms. At $R=R_2\approx R_1+p^2(\pi^6-3\alpha^4\pi^2-2\alpha^6)/\alpha^4$ the rolls with wave vector $\{\alpha,0\}$ bifurcate from the equilibrium. The corresponding fixed point

$$a_1=a_3=u=0,\quad a_2^2=\gamma_2(R-R_2)\sigma_{22}^{-1} \tag{5.4}$$

in the phase space has a two-dimensional unstable manifold. Just as in the case of the NWS equation, the respective in-

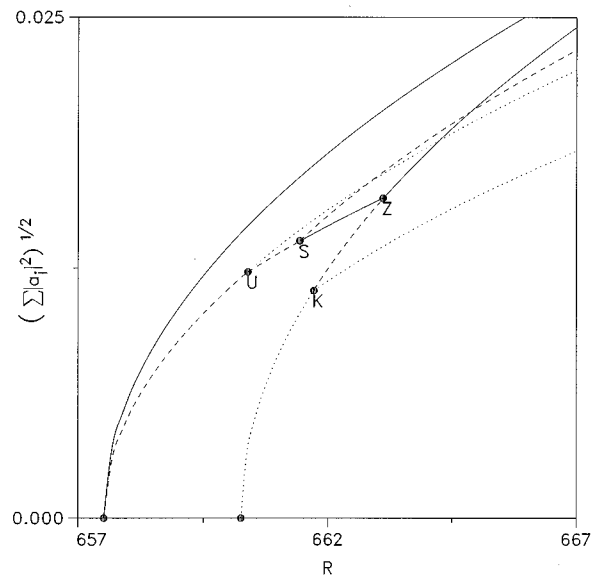


FIG. 6. Exchange of stability between steady convection solutions for $P=5$, $\alpha=2.1$, $p=\sqrt{\alpha_c^2-\alpha^2}=0.724$. Stable solutions are indicated by solid lines, unstable solutions with one (two) positive growth rates are indicated by dashed (dotted) lines. The circles mark the same pitchfork bifurcation as in Fig. 2. In addition, the bifurcation $Z$ which marks the transition from undulating to straight rolls with increasing $R$ is shown.

stabilities correspond either to deformations of the roll boundaries (zigzags) or to amplitude modulations (knuckles). When the value $R_K$ of $R$ satisfying the condition

$$\gamma_1(R-R_1)\sigma_{22}\equiv\gamma_2(R-R_2)(\sigma_{12}+\sigma_{14}), \tag{5.5}$$

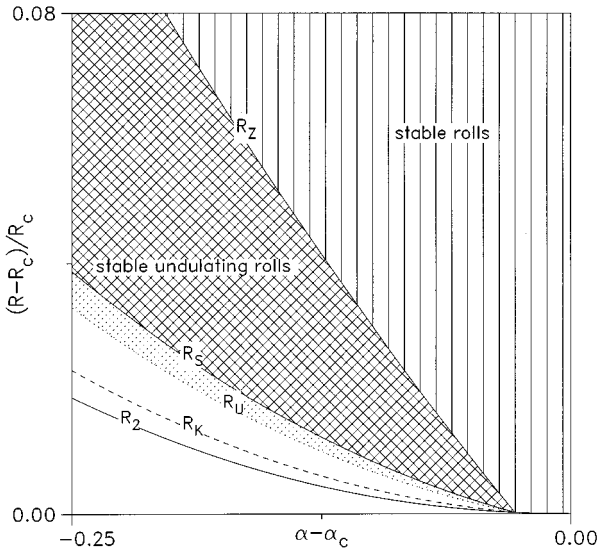


FIG. 7. Bifurcation lines and stability regions in the case $P=50$, $p=0.5$. The meaning of the symbols is as follows: $R_2$, birth of rolls (unstable for $q<-0.027\,99$); $R_U$, birth of unstable zigzags from unstable rectangles; $R_K$, removal of the knuckle instability for the rolls; $R_S$, stabilization of undulating rolls through symmetry breaking; $R_Z$, removal of zigzag instability for rolls.

which for small $p$ is

$$R=R_K=R_1+\tfrac{3}{2}(R_2-R_1)+o(p^3), \tag{5.6}$$

is reached, the knuckle instability is removed via the subcritical bifurcation: The resulting steady solutions with $u=0$, $a_1=a_3$ are unstable everywhere in the domain of their existence, $R>R_K$. The further increase of $R$ leads to the next bifurcation at $R=R_U$ which corresponds to

$$\gamma_2(R-R_2)(\sigma_{11}+\sigma_{13})=\gamma_1(R-R_1)(2\sigma_{21}-\sigma_{24}-4p^2Qs_2), \tag{5.7a}$$

i.e.,

$$R=R_U=R_1+(R_2-R_1)\,\frac{3P^2\alpha^2}{3P^2\alpha^2+4\pi^2(1+P)}+o(p^3). \tag{5.7b}$$

At this point the undulating roll solutions with

$$\begin{aligned}
a_1^2&=[\,\gamma_1(R-R_1)\sigma_{22}-\gamma_2(R-R_2)(\sigma_{12}-\sigma_{14}\\
&\quad+2p^{-2}s_1Q)]\Delta^{-1},\\
a_2^2&=[\,\gamma_2(R-R_2)(\sigma_{11}+\sigma_{13})-\gamma_1(R-R_1)(2\sigma_{21}-\sigma_{24}\\
&\quad-4p^{-2}s_2Q)]\Delta^{-1},\\
a_3&=-a_1,\\
u&=-2p^2Qa_1a_2,
\end{aligned} \tag{5.8}$$

where

$$\begin{aligned}
\Delta&=(\sigma_{11}+\sigma_{13})\sigma_{22}-(\sigma_{12}-\sigma_{14}+2p^{-2}s_1Q)\\
&\quad\times(2\sigma_{21}-\sigma_{24}-4p^{-2}s_2Q)
\end{aligned}$$

branch from the unstable rectangles. The solutions (5.8) inherit from the rectangular pattern the instability with respect to perturbations which violate the symmetry $a_3=-a_1$. This instability is removed by the subcritical pitchfork bifurcation which occurs at $R=R_S$ when the coefficients of (5.2) satisfy

$$\gamma_1(R-R_1)=a_1^2(3\sigma_{11}-\sigma_{13})+a_2^2(\sigma_{12}+\sigma_{14}), \tag{5.9}$$

where the values of $a_1$ and $a_2$ are taken from (5.8). For small $p$ this expression yields

$$\begin{aligned}
R_S&\approx R_2+(R_2-R_1)\\
&\quad\times\frac{3P^4\alpha^4-6P^2\alpha^2\pi^2(1+P)+4\pi^4(1+P)^2}{P^4\alpha^4+5P^2\alpha^2\pi^2(1+P)-4\pi^4(1+P)^2}.
\end{aligned} \tag{5.10}$$

This symmetry-breaking bifurcation produces unstable steady solutions with $a_3\neq-a_1$ which exist in the parameter domain $R>R_S$. Finally the value of the Rayleigh number

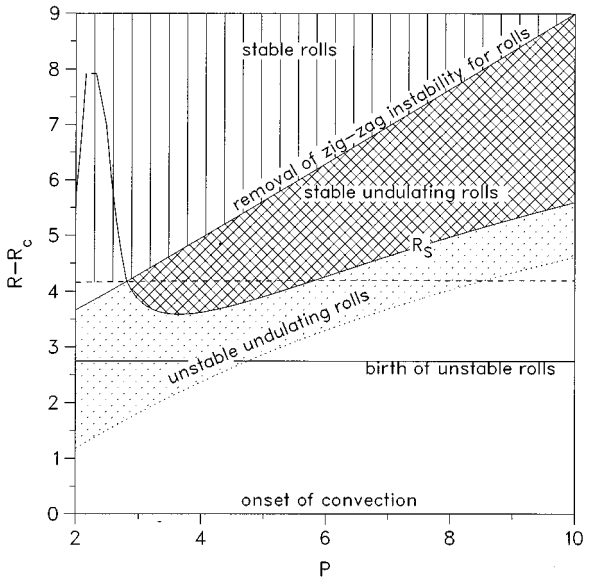


FIG. 8. Dependence of stability boundaries on the Prandtl number for the horizontal periodicity interval given by $\alpha=2.1$, $p=0.724$.

reaches the boundary of the zigzag instability $R=R_Z$ which is determined by the condition

$$\gamma_1(R-R_1)\sigma_{22}=\gamma_2(R-R_2)(\sigma_{12}-\sigma_{14}+2p^{-2}Qs_1). \quad (5.11)$$

For small $p$ the latter becomes

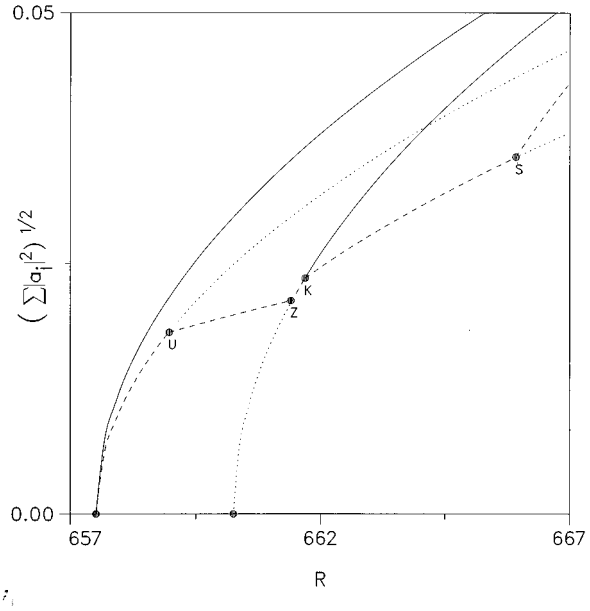


FIG. 9. Stability exchange for the low values of $P,P=2.4$. The same wave vectors as in Figs. 6 and 7 have been chosen. Stable solutions are indicated by solid lines, unstable solutions with one (two) positive growth rates are indicated by dashed (dotted) lines. The circles mark the same bifurcations as Figs. 2 and 6, but the symmetry-breaking bifurcation $S$ occurs for the knuckle solution instead of the modulating rolls.

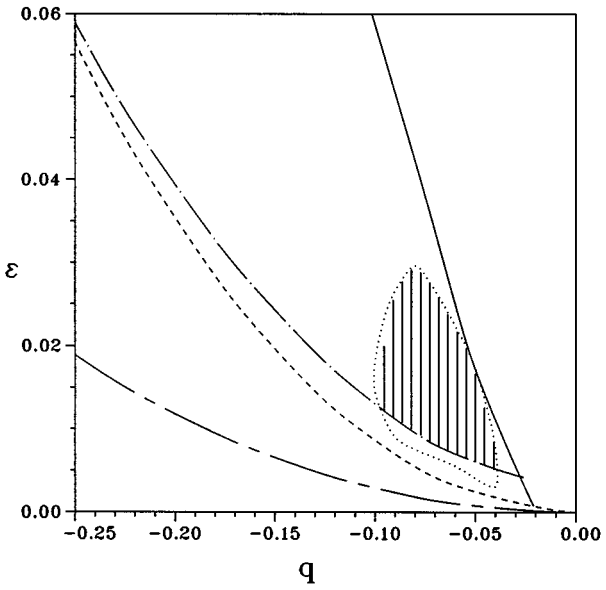


FIG. 10. The stability of flows for $p=0.5$ and $P=100$ as a function of the scaled supercritical Rayleigh number $\varepsilon$ and the wave number $q$. Primary rolls, which exist above the neutral curve (long-dash short-dashed line), are stable above the zigzag line (——) or the Eckhaus line (---) depending on which one is higher. Undulating rolls are stable in the hatched region and undergo instability with respect to domain modes (-·-·-) or with respect to undulation modulations (·····).

$$R_Z=R_2+(R_2-R_1)\frac{\alpha^2P^2}{2\pi^2(1+P)}+o(p^3). \quad (5.12)$$

Here the stable undulating rolls (5.8) merge with the unstable straight rolls (5.4), transferring to the latter their stability: for $R>R_Z$ the pattern (5.4) is stable. It is straightforward to see that for $\alpha\to\pi/\sqrt{2}$ the last expression provides the boundary (2.5a) [18,22]. The stability exchange between the steady

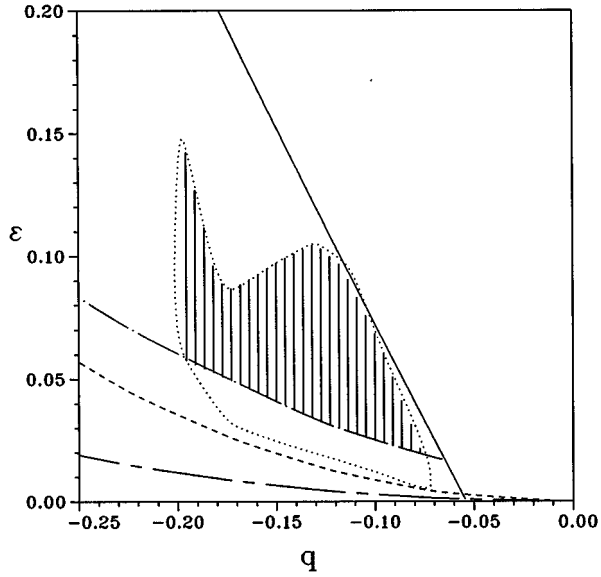


FIG. 11. Same as Fig. 10, but for $p=0.7$ and $P=100$.

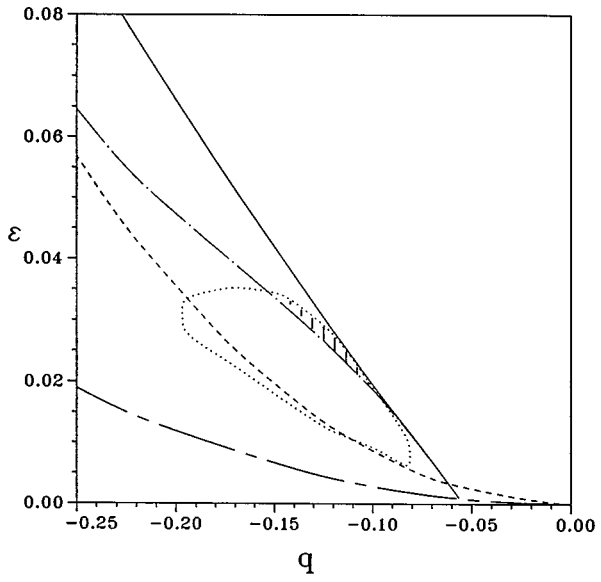


FIG. 12. Same as Fig. 10, but for $p=0.7$ and $P=25$.

solutions of Eq. (5.2) caused by the increase of $R$ under the fixed values of $\alpha=2.1$, $p=0.7$, $P=5.5$ is presented in Fig. 6. The relatively low value of $P$ has been chosen in order to enhance the resolution of the plotted curves which can otherwise hardly be distinguished. The phase diagram in the plane of the parameters $q=\alpha-\alpha_c$ and $R$ for the fixed values $P=50$ and $p=0.5$ is shown in Fig. 7.

As in the case of the NWS equation, the stability domain of the undulating rolls in the $\varepsilon$-$q$ plane lies between two curves, marking the onset of the symmetry-breaking instability and of the zigzag instability, respectively. The only difference is the location of the latter curve. In the NWS type analysis this boundary on the $q$-$\varepsilon$ plane is parallel to $q=0$ [up to the effects associated with a nonvanishing $c(P)$, see (2.5b) and (2.5c) above]; hence the increase of $\varepsilon$ alone leaves the roll pattern unstable with respect to zigzag perturbations. In the presence of the mean flow, however, the increase of $R$ leads to the disappearance of the zigzag mode, and the resulting boundary in Fig. 7 is inclined.

As the value of the Prandtl number is decreased, the whole sequence of events is altered. The boundary of the knuckle instability is almost insensitive to variations of $P$. The latter mainly affects the intensity of the mean flow. But as can be seen from the shape of the knuckle pattern (Fig. 1), the curvatures of the opposite sides of the roll exactly balance each other. Hence the bifurcating unstable steady solution does not include a mean flow component. On the other hand, bifurcations associated with the undulating roll pattern are strongly affected by changes of $P$: the graphs of $R_U(P)$, $R_S(P)$, and $R_Z(P)$ on the parameter plane follow the decrease of $P$ (see Fig. 8 for $\alpha=2.1$ and $p=0.724$).

The bifurcation curves $R_Z(P)$ and $R_K(P)$ intersect in the point, the coordinates $P_*$ and $R_*$ of which ensure $\sigma_{14}=p^{-2}s_1Q$. For small $p$ this equality can be transformed with the help of (5.3) into

$$\frac{P_*^2}{P_*+1}=\frac{\pi^2}{\alpha^2}. \tag{5.13}$$

For $P<P_*$ the order of bifurcations following the increase of $R$ from $R_2$ is different (Fig. 9): now the first instability of the pattern (5.4) to be removed is the zigzag instability. The undulating rolls (5.8) are unstable towards the symmetry-breaking perturbations everywhere in the domain of their existence, $R_U(P)<R<R_Z(P)$. Immediately beyond the boundary of the zigzag instability the straight rolls (5.4) are still unstable with respect to the knuckle mode. Their stability is completely restored on reaching the line $R=R_K(P)$. The knucklelike steady solutions produced by this bifurcation are always unstable. The further growth of $R$ increases the number of their instabilities, when the two steady solutions with $a_1\neq a_3$ branch from the knuckle mode as a consequence of the symmetry-breaking bifurcation as shown, for instance, at the point $S$ in Fig. 9. This instability is analogous to the corresponding instability of the undulating rolls and is also described by expression (5.9). The branch of the traveling-wave solutions which results from the interaction of the zigzag and the knuckle instabilities bifurcates into the direction $P<P_*$ and is unstable. Thus stable undulating rolls can be met only for $P>P_*$. The value of $P_*$ depends on $\alpha$ and $p$. Keeping in mind that $\alpha^2\leqslant\alpha_c^2=\pi^2/2$, we see from (5.13) that the value $P=1+\sqrt{3}=2.732\ldots$ represents the lowest possible boundary of $P_*(\alpha,p)$.

## VI. LONG-WAVE INSTABILITIES AND THEIR NONLINEAR EVOLUTION

In order to investigate the stability of undulating rolls with respect to wavelength changing instabilities at finite Prandtl numbers we have extended the system of Eq. (5.1) to one with at least nine wave vectors included. The coefficients have been calculated numerically from the underlying basic equations (2.1) by assuming that all rolls have approximately the same critical Rayleigh number, i.e., we have a multiple bifurcation point. The computations confirmed that in the parameter space the region of stability for the undulating rolls lies between the boundary of the ''domain'' instability and the border of the longitudinal modulation instability.

The results of the analysis can be seen in Figs. 10 and 11 for $P=100$ and $p=0.5$ or 0.7, respectively. In comparison with the case of infinite $P$ (see Fig. 4), the region of stable undulations is much bigger for this intermediate value of $P$. The region of stable undulations also grows with increasing $p$. The deformation of the stability boundary in the case of $P=100$, $p=0.7$ seems to be due to a Prandtl number effect. When the Prandtl number is decreased further, the region of stability shrinks again, as can be seen in Fig. 12 for which the parameters $P=25$ and $p=0.7$ were chosen. This effect is due to the decreasing regime of stable zigzags with respect to the symmetry-breaking instability for decreasing $P$ analyzed in Sec. V and shown in Fig. 8.

Although the domain instability may be viewed as a wave number adjustment process [14], it conserves the number of the roll pairs in contrast to the classical Eckhaus instability. The computations confirm the supercritical character of the respective bifurcation. The stability of the domain states was checked by the time integration of the corresponding equations with the use of the explicit Adams-Bashforth method. The initial conditions for most of the runs were chosen near

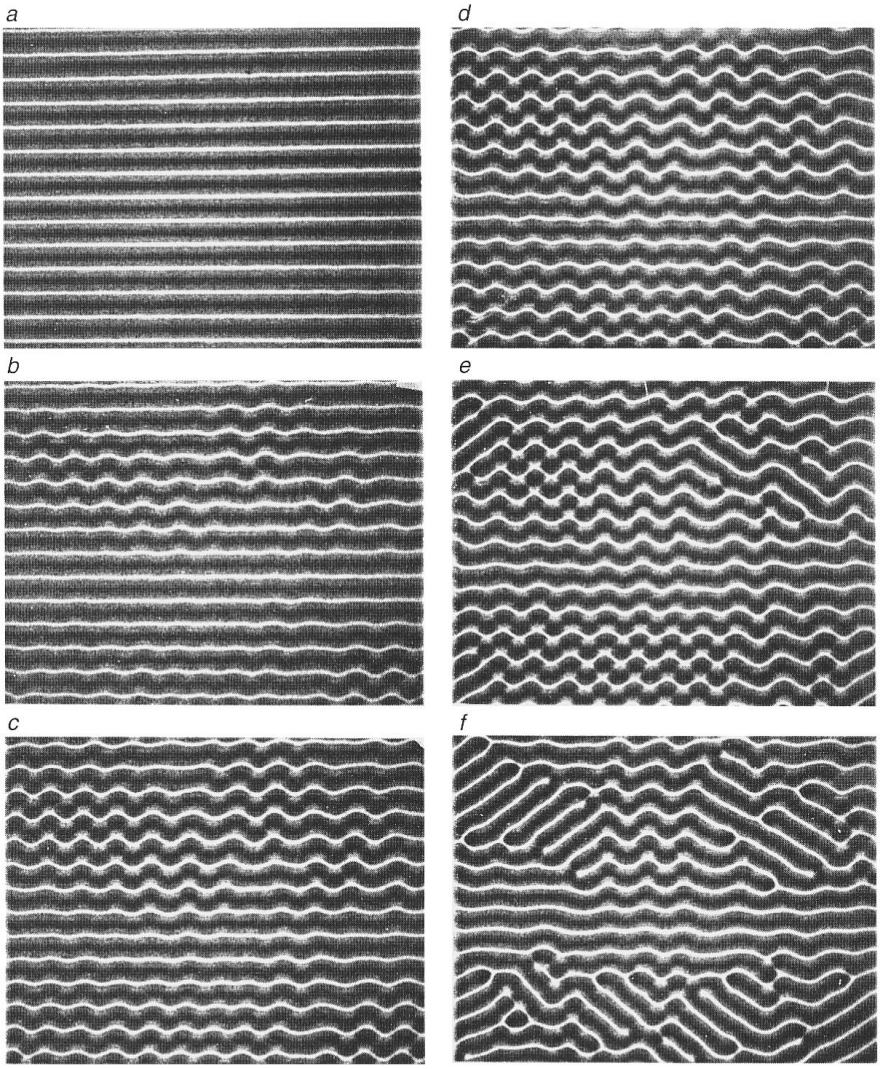


FIG. 13. Shadowgraph visualization of the evolution of the zigzag instability in a layer of silicone oil heated from below. Intervals between the photographs are about 10 min except for the last interval, which is about 30 min. The same parameter values ($R \approx 3600$, $P \approx 100$) as in the case of Fig. 11 of Ref. [13] were used.

the slightly distorted roll pattern (under the parameter values where this pattern is unstable with respect to the zigzag perturbations). Usually the system heads for the undulating pattern. If the latter is also unstable, further instabilities evolve. For higher orders of truncation we also used the vicinity of the steady undulating roll solution as a starting point.

It can be seen that the domain pattern is stable for truncations including nine and more wave vectors, although the increase of the number of modes leads to some decrease of the stability region. It turns out that adding the modes whose wave numbers are multiples of the undulation wavelength does not influence the stability. Much more dangerous for the domain pattern with the transversal modulation wave number $d$ are the subharmonic disturbances corresponding to the modes with $(2n-1)d/2$, $n=1,2,\ldots$. When initial conditions near the primary roll are chosen, the domain mode with the smallest possible wave vector is usually reached as a stable fixed point. But a detailed study of the preferred wavelength of the domain pattern as a function of the parameters of the problem has not yet been made.

## VII. DISCUSSION

The theoretical predictions made in this paper and the preceding Letter [14] could eventually be tested in a laboratory experiment. The method of controlled initial conditions introduced by Chen and Whitehead [23] and applied successfully in the experimental study [13] of the stability of roll pattern in dependence on their wavelength could be used to explore stable patterns of undulating rolls and of domain structures together with their instabilities. At the time of the earlier study [13] there were no theoretical reasons to attempt a more detailed exploration of the parameter space. Nevertheless, the observations did indicate a tendency towards domain formation. In Fig. 13 a previously unpublished set of the photographs is shown, obtained in the same fashion as those given in Ref. [13]. Through controlled initial conditions rolls with a wavelength in the zigzag-unstable regime were generated. As the zigzag instability evolves, it spreads primarily along the axis of the rolls and tends to compress rolls between regions of strong undulations such that an intermediate region of only weakly undulating rolls is obtained. In the case of Fig. 13, the parameters were obviously chosen in such a way that the strongly undulating rolls evolved into oblique rolls. But the tendency towards a domain structure is noticeable in that the weakly undulating rolls return to almost straight rolls.

The main difference between the laboratory apparatus and the assumptions of the theory is the finitely conducting

boundaries of the experimental configuration. Because of the use of the shadowgraph method for the visualization, this condition will probably be retained in future experiments. But all indications suggest that only qualitative aspects of the experiment such as a shift in the critical value of the wave number will be affected by a finite ratio between the conductivities of fluid and boundary. Since the case of undulating rolls seems to be the only case for which theoretical predictions on pattern domains are available, future experiments are highly desirable.

## ACKNOWLEDGMENT

The research reported in this paper has been supported by the Deutsche Forschungsgemeinschaft.

[1] D. Avsec and M. Luntz, Météorologie **31**, 180 (1937).
[2] H. Bénard and D. Avsec, J. Phys. Radium **9**, 486 (1938).
[3] J. E. Hart, J. Fluid Mech. **48**, 265 (1971).
[4] A. Joets and R. Ribotta, *Cellular Structures in Instabilities*, edited by J. E. Wesfreid and S. Zaleski (Springer-Verlag, New York, 1984), p. 294; R. Ribotta, A. Joets, and Lei Lin, Phys. Rev. Lett. **56**, 1595 (1986).
[5] R. M. Clever, F. H. Busse, and R. E. Kelly, J. Appl. Math. Phys. (Zeitschrift für angewandte Mathematik und Physik) **28**, 771 (1977).
[6] R. M. Clever and F. H. Busse, J. Fluid Mech. **81**, 107 (1977).
[7] R. M. Clever and F. H. Busse, J. Fluid Mech. **229**, 517 (1991).
[8] E. Bodenschatz, M. Kaiser, L. Kramer, W. Pesch, A. Weber, and W. Zimmermann, in *New Trends in Nonlinear Dynamics and Pattern-Forming Phenomena*, edited by P. Coullet and P. Huerre (Plenum, New York, 1990), pp. 111–124.
[9] R. E. Kelly, Adv. Appl. Mech. **31**, 35 (1994).
[10] A. Schlüter, D. Lortz, and F. H. Busse, J. Fluid Mech. **23**, 129 (1965); F. H. Busse, Ph.D. dissertation, University of Munich, 1962 [English translation by S. H. Davis, Rand Corporation Report No. LT-66-19, 1966 (unpublished)].
[11] F. H. Busse, J. Math. Phys. **46**, 140 (1967).
[12] F. H. Busse, Rep. Prog. Phys. **41**, 1929 (1978).
[13] F. H. Busse and J. A. Whitehead, J. Fluid Mech. **47**, 305 (1971).
[14] F. H. Busse and M. Auer, Phys. Rev. Lett. **72**, 3178 (1994).
[15] F. H. Busse, in *Proceedings of the International Union of Theoretical and Applied Mechanics Symposium Herrenalb, 1969, Instability of Continuous Systems*, edited by H. Leipholz (Springer, New York, 1971), pp. 41–47.
[16] R. M. Clever and F. H. Busse, J. Fluid Mech. **65**, 625 (1974).
[17] P. Manneville and J. M. Piquemal, Phys. Rev. A **28**, 1774 (1983).
[18] E. D. Siggia and A. Zippelius, Phys. Rev. Lett. **47**, 835 (1981).
[19] A. C. Newell and J. A. Whitehead, J. Fluid Mech. **38**, 279 (1969).
[20] L. A. Segel, J. Fluid Mech. **38**, 203 (1969).
[21] F. H. Busse, M. Kropp, and M. Zaks, Physica D **61**, 94 (1992).
[22] F. H. Busse and E. W. Bolton, J. Fluid Mech. **146**, 115 (1984).
[23] M. M. Chen and J. A. Whitehead, J. Fluid Mech. **31**, 1 (1968).